Intensification of an eddying Southern Ocean Meridional Overturning due to the Southern Annular Mode

Carolina O. Dufour, Julien Le Sommer, Jan D. Zika, Marion Gehlen, Pierre Mathiot, Bernard Barnier

Intensification of an eddying Southern Ocean Meridional Overturning due to the Southern Annular Mode

C.O. Dufour *

Laboratoire des Ecoulements Géophysiques et Industriels, CNRS/UJF/INPG, France

Laboratoire des Sciences du Climat et l'Environnement, CEA/CNRS, France

J. Le Sommer , J.D. Zika

Laboratoire des Ecoulements Géophysiques et Industriels, CNRS/UJF/INPG, France

M. Gehlen

Laboratoire des Sciences du Climat et l'Environnement, CEA/CNRS, France

P. Mathiot

Université catholique de Louvain, Institut d'astronomie et de géophysique Georges Lemaître, Belgium

B. Barnier

Laboratoire des Ecoulements Géophysiques et Industriels, CNRS/UJF/INPG, France

ABSTRACT

Realistic regional simulations at eddying to eddy-resolving resolutions are used to investigate the role of the Southern Annular Mode (SAM) in the dynamics of the Southern Ocean. A series of sensitivity experiments are run with two synthetic interannual forcings. They correspond, on the one hand, to homogeneously intensified winds, and on the other hand to poleward intensified winds consistent with an increase in the SAM. As expected, eddies are found to mitigate the response of the Antarctic Circumpolar Current (ACC) and Meridional Overturning Circulation (MOC) to poleward intensified winds. However it is not necessarily the case that transient eddies play an increasing role with increasing winds and resolution. It is found that, as winds increase, meridional transports due to transient eddies can decrease while standing eddy transports become more efficient at balancing the wind induced overturning. In one case the role of transient eddies in the MOC reduces to almost zero. This presents new challenges for eddy flux parameterization. In addition, the ocean dynamical response induced by homogeneous wind anomalies present essential differences from those induced by poleward intensified wind anomalies. In particular, poleward intensified wind anomalies are far more efficient in accelerating the ACC than homogeneous wind anomalies. The spatial pattern of wind anomalies is found to be crucial in the Southern Ocean dynamical response to wind changes.

* *Corresponding author address:* Carolina Dufour, Laboratoire des Ecoulements Géophysiques et Industriels, CNRS/UJF/INPG, BP53, 38041 Grenoble cedex 9, France.

E-mail: carolina.dufour@hmg.inpg.fr

1. Introduction

The Southern Annular Mode (SAM) is the dominant mode of atmospheric variability in the Southern Hemisphere. This mode of variability is characterized by an annular structure centered over Antarctica and appears in many atmospheric fields. Positive phases of the SAM correspond to a contraction of the circumpolar vortex which results in poleward-intensified zonal winds over the circumpolar ocean (Hall and Visbeck 2002; Sen Gupta and England 2006). Historical observations show a trend in the SAM towards its positive phases over the past decades (Thompson et al. 2000; Cai and Whetton 2003; Marshall 2003). This positive trend in the SAM has been shown to be a non-linear combination between natural and anthropogenic forcing (Thompson and Solomon 2002; Marshall et al. 2004).

The Southern Ocean is known to be a major sink of carbon dioxide (Metzl et al. 1999; Le Quéré et al. 2007). The response of the Southern Ocean carbon cycle to the upward trend in the SAM is thought to be driven at first order by the response of upwelling bringing DIC-rich water to the surface (Lenton and Matear 2007; Lovenduski et al. 2007, 2008), and hence, by the response of the meridional overturning circulation (MOC).

The MOC cannot be directly deduced from observations and must be indirectly inferred. Modeling studies offer the opportunity to assess the expected response of the MOC to changes in winds. Following a poleward intensification of zonal winds, an increase and poleward shift in meridional Ekman transport and Ekman pumping is expected. This shift would be followed by tightening of isopycnal slopes resulting in both an intensification and a poleward shift of the transport of the Antarctic Circumpolar Current (ACC) (Hall and Visbeck 2002; Spence et al. 2010). In such a case, the MOC is likely to be enhanced and shifted as well (Sen

Gupta and England 2006; Hallberg and Gnanadesikan 2006). Many recent modeling studies have shown, for a positive phase of the SAM, both an increase in vertical tilt of isopycnals inducing a more intense ACC (Hall and Visbeck 2002; Meredith and Hogg 2006; Yang et al. 2008; Spence et al. 2010; Farneti et al. 2010) and a southward shift of the ACC by a few degrees (Spence et al. 2010). The MOC is also found to intensify and its structure is found to be strongly affected by poleward intensifying winds thus implying significant changes in water masses properties and their rate of formation (Oke and England 2004; Sen Gupta and England 2006; Hallberg and Gnanadesikan 2006).

Recent observed trends in isopycnal slopes suggest that the transport in the ACC and meridional overturning in the Southern Ocean may be insensitive to decadal changes in wind stress (Böning et al. 2008). Also, some recent studies using high resolution models have shown that transient eddies may play a major role in the dynamical response of the Southern Ocean to the SAM. Indeed, transient eddies are thought to counteract the steepening of isopycnal slopes induced by the increase in Ekman transport. In particular, such a compensation is to be expected if the Southern Ocean is in an eddy-saturated state as suggested by Straub (1993) and Hogg et al. (2008). In an eddy-saturated state, an increase in wind stress does not significantly change the transport of the ACC, but instead enhances the eddy field. Hogg (2010) even recently suggested that, in such an eddy-saturated state, the circumpolar transport is independent of wind stress and is rather driven by buoyancy forcing. The response of the MOC to changes in winds was also found to be significantly moderated by eddies (Hallberg and Gnanadesikan 2006; Farneti et al. 2010).

It has thus been proposed that the apparent discrepancy between the results of coarse resolution models and the limited observations, is due to the ability of models to accurately

resolve eddies or not. Resolving eddies (and not only parameterizing their effect) appears to be crucial when studying the response of the Southern Ocean to changes in the SAM. However, modeling studies at fine resolution have largely considered idealized changes in wind patterns and not changes consistent with the pattern of the SAM. Some of the discrepancy between coarse and fine resolution studies simulating the response of the ocean to the SAM may be due to the representation of the SAM forcing itself.

Modeling studies carrying out sensitivity experiments to the SAM forcing tend to fall into two camps: coarse resolution studies with "realistic" changes in the SAM (Lefebvre and Goose 2005, i.e. both intensification and poleward shift of winds) and fine-resolution models with highly idealized changes (Oke and England 2004; Hallberg and Gnanadesikan 2006; Klinger and Cruz 2009, i.e. a homogeneous intensification or a poleward shift in the winds). Some recent modeling studies have attempted to bridge this gap, with SAM like forcing changes in models at coarse to eddying resolutions with Farneti et al. (2010) and Spence et al. (2010). However, there remains a need to understand the difference between a homogeneous increase in Southern Hemisphere winds and changes in the winds consistent with the SAM, in both eddy-permitting and eddy-resolving regimes.

In this paper, we thus address the dynamical response of the Southern Ocean to the SAM with a particular focus on (i) how eddies affect this response and (ii) to what extent the spatial representation of the SAM matters in this response. We use simulations of the Southern Ocean at both eddy-permitting and eddy-resolving resolutions. A series of sensitivity experiments to Southern Hemisphere wind intensity and pattern is carried out. The response of the ACC transport and the MOC to winds intensified homogeneously over the whole Southern Ocean on the one hand, and to intensified-winds regressed onto the

observed SAM pattern on the other hand, is investigated.

The rest of the paper is set out as follows: the series of sensitivity experiments is presented in Section 2 along with details on the model used. Response of the ACC transport and the MOC to changes in winds is shown in Section 3. Section 4 discusses the response of the MOC in a particular SAM regime. A summary and conclusions are given in Section 5.

2. Methods

a. Ocean model

In this study, we use the modeling system NEMO (*Nucleus for European Modeling of the Ocean*, Madec (2008)) which couples the hydrostatic, primitive equation ocean model OPA (Madec et al. 1999) with the Louvain-la-Neuve sea-ice model LIM (Fichefet and Maqueda 1997). The atmospheric forcing is the Drakkar Forcing Set 3 (DFS3) and is built from a combination of ERA-40 (until year 2001) and ECMWF variables (from year 2002, for air temperature and humidity, 10-m winds) and satellite observations (for precipitations and radiations), as described in Brodeau et al. (2010).

Simulations performed in this study are part of a hierarchy of models developed during the DRAKKAR project (Drakkar Group 2007). Here, we use a regional extraction from the DRAKKAR global configurations *ORCA*, including all the ocean south of 30°S and called *PERIANT*. This model configuration is run at both a horizontal resolution of 0.5° (PERIANT05) and 0.25° (PERIANT025) on a Mercator grid. There are 46 vertical levels with a grid spacing finer at the surface (6 m) and increasing with depth to 250 m at the bottom.

Table 1 compares grid types and grid sizes at 60°S from various state-of-the-art model configurations used in similar studies on the Southern Ocean sensitivity to winds. To ensure the ease of comparison between simulations at 0.5° and 0.25° horizontal resolutions, no eddy induced advection parameterization, such as that of Gent and McWilliams (1990), is used in the simulations discussed in this paper. The vertical mixing is represented with the TKE scheme with a background vertical mixing coefficient of $10^{-5} m^2.s^{-1}$ (Madec 2008).

In PERIANT05 and PERIANT025 regional configurations, the northern boundary at 30°S is open and forced under radiation conditions (Treguier et al. 2001) with the outputs of the corresponding DRAKKAR global simulations ORCA05-G70 and ORCA025-G70, respectively (Barnier et al. 2006; Biastoch et al. 2008). Those global simulations have been proven "realistic" (e.g. Lombard et al. 2009) in particular in the Southern Ocean (Renner et al. 2009; Treguier et al. 2007).

For all simulations, the ocean starts at rest and temperature and salinity are initialised with the NODC (Levitus) World Ocean Atlas 1998. The period chosen to run the simulations is 1980-2004, since it is doubtful that atmospheric reanalyses correctly reproduce the interseasonal variability of Southern Ocean winds in the pre-satellite era (Bromwich and Fogt 2004). In the rest of the paper, analyses are carried out over the period 1995-2004. This corresponds to a spin-up of 15 years allowing the circulation to be well stabilized (see Fig. 3).

A typical issue in fine resolution ocean models is their inability to capture the descent of Antarctic Bottom Water (AABW, Winton et al. 1998; Lee et al. 2002). This can result in a slow downward trend in ACC transport and is the case in ORCA05 and ORCA025 global configurations, of which PERIANT05 and PERIANT025 are regional extractions (Treguier

et al. 2010). To overcome this issue, many models employ 3D relaxation of water mass properties towards a climatology to ensure the presence of deep waters at the ocean bottom (e.g. Hallberg and Gnanadesikan 2006). A 3D relaxation of AABW towards the NODC (Levitus) World Ocean Atlas 1998 is used in all our simulations. A precise description of the method used is presented in the Appendix.

b. Synthetic forcing

For both horizontal resolutions, we have performed simulations designated as follows: REF, which refers to control experiments where the atmospheric reanalysis winds are unperturbed; WIND, which refers to sensitivity experiments where the winds are increased homogeneously; and SAM, which refers to sensitivity experiments where winds are perturbed according to the observed pattern of the SAM. We now describe how the synthetic forcing for the WIND and SAM experiments is constructed.

The ocean model forcing depends, to a large degree, on the wind velocity at 10 m in the atmosphere, $\mathbf{U}(x, y, t)$. In the REF experiments, this 10 m wind velocity is simply that of the atmospheric reanalysis ($\mathbf{U}_{ar}(x, y, t)$). In the WIND experiments, the magnitude of $\mathbf{U}$ is permanently and homogeneously increased over the domain. In the SAM experiments, a pattern $\mathbf{P}_{U_{ar}}$ which describes the spatial wind anomaly pattern of the SAM is permanently added. Hence the general formula for $\mathbf{U}$ may be written:

$$\mathbf{U}(x, y, t) = \alpha \mathbf{U}_{ar}(x, y, t) + \beta \mathbf{P}_{\mathbf{U}_{ar}}(x, y). \tag{1}$$

Above, α and β are constants. Following Lefebvre and Goose (2005), $\mathbf{P}_{\mathbf{U}_{ar}}$ is the regression pattern of $\mathbf{U}_{ar}$ onto the SAM index, I_{SAM}, such that:

$$(\mathbf{U}_{ar}(x,y,t) - I_{SAM}(t) \cdot \mathbf{P}(x,y))^t (\mathbf{U}_{ar}(x,y,t) - I_{SAM}(t) \cdot \mathbf{P}(x,y)) \quad (2)$$

is minimized over the period 1980-2001 and over the model domain (South of 30°S). The index I_{SAM} is the 1980-2001 monthly SAM index built from NCEP products[1].

Fig. 1.a shows the zonal component of the regression pattern, $\mathbf{P}_{\mathbf{U}_{ar}}$, onto the SAM index. The pattern holds a very zonal structure with positive coefficients in the southern regions where the ACC stands (around 60°S) and negative coefficients on the north side of the Southern Ocean. This pattern indeed corresponds to a poleward intensification of zonal winds over the circumpolar ocean and a weakening of zonal winds farther north, for a positive phase of the SAM, as described by many authors (e.g. Hall and Visbeck 2002; Sen Gupta and England 2006).

The WIND experiments correspond to the strategy of forcing used by Hallberg and Gnanadesikan (2006), except that the wind velocity is modified instead of the wind stress. The use of bulk formulation as ocean surface boundary condition in our model implies that the wind velocity enters in the calculation of wind stress, transfer coefficient for momentum, evaporation and sensible and latent heat. This leads to the fact that i) while we only modify the mechanical part of the forcing (wind velocities), the thermodynamic part of the forcing is also partly affected via surface fluxes and ii) although we do not use a coupled ocean-atmosphere model, bulk formulation allows a feedback from the ocean to the atmosphere via surface fluxes. The SAM experiments correspond to the strategy of forcing used by Lefebvre and Goose (2005). However, Lefebvre and Goose (2005) built a series of synthetic forcings where wind stress and air temperature were perturbed separately. We leave the air

[1] see $http://www.cpc.ncep.noaa.gov/products/precip/CWlink/daily_ao_index/aao/monthly.aao.index.b79.current.ascii$

temperature unperturbed in all experiments.

Based on the above method, a series of experiments are performed whose characteristics are summarized in Table 2. For each type of synthetic forcing (ie WIND and SAM forcings), three simulations with increasing intensity in wind anomaly (symbolized by one, two or three crosses in simulation names) are run at 0.5° resolution. Only the simulations with the strongest wind anomaly of each type of synthetic forcing are run at 0.25° resolution, for computational cost reasons. The linearity of the Southern Ocean response to changes in wind is only studied for the 0.5° simulation set.

Fig. 1.b shows the 1995-2004 zonal profiles of wind stress for the series of 0.5° experiments. WIND simulations have maxima at the same latitude as the control simulation, whereas the SAM simulations maxima are shifted poleward by roughly 3°, simulating the poleward shift of zonal winds during positive phases of the SAM. In the WIND simulations, the wind velocity is increased by either 10%, 20% or 30% so that the mean zonal wind stress is doubled[2] in the WIND05+++ simulation. In the SAM simulations, the mean zonal wind stress increase is lower and reaches a maximum of 1.5 of the REF05 simulation value.

c. Consistency of model simulations

The spatial patterns from 1992-2002 averaged Eddy Kinetic Energy (EKE) in the REF05 and REF025 simulations are compared to the observations in Fig.2. Observational estimates of EKE come from TOPEX/Poseidon 1992-2002 data set. The most energetic regions are found in the latitude band corresponding to the ACC as well as in the Agulhas current, the

[2]Wind stress is a quadratic function of the wind velocity

Brazil-Malvinas confluence and the south-eastern side of Australia. Whatever the resolution of simulations, regional patterns are generally in very good agreement between model and observations. Zonally integrated near-surface EKE averaged between 35° and 65°S for the period 1992-2002 is 27 $cm^2.s^{-2}$ for REF05 and 69 $cm^2.s^{-2}$ for REF025, corresponding to roughly one-fourth and two-thirds of observed values, respectively. Therefore, REF05 and REF025 slightly underestimate the EKE, although the EKE representation is notably improved when increasing resolution.

Fig. 3 shows the time series of the annual mass transport at Drake Passage in REF05 and REF025 regional simulations, and in their corresponding global simulations. Regional simulations are run from 1980 to 2004 period while global simulations are run from 1958 to 2004. The regional simulations show a spin-up of 8 years and no more trend appears afterwards while the global simulations show a spin-up of roughly 15 years and keep a slow downward trend afterwards. This is due to the 3D relaxation of AABW (see Appendix) which was applied to regional simulations only. The 3D relaxation maintains the deep meridional gradient of density in the Southern Ocean thus stabilising the ACC transport. As a consequence, the transport is more intense in regional simulations than in global simulations by at least 10 Sv (Sv = 10^6 $m^3 s^{-1}$). In REF05 and REF025, the averaged transport at Drake Passage over the final ten years (period 1995-2004) is 142.6 Sv and 143.2 Sv, respectively. These are typical values for transport through Drake Passage, observations giving values ranging from 110 Sv to 150 Sv (Whitworth 1983; Whitworth and Peterson 1985; Cunningham et al. 2003). Moreover, it is worth noting that transports at Drake Passage differ by only a few Sv between REF05 and REF025. Previous studies show ACC transports that differ by tens of Sv depending on model resolution (e.g. Hallberg and Gnanadesikan 2006; Farneti et al. 2010).

Fig. 4 shows the mean 1995-2004 salinity along the 115°E section of the Southern Ocean in the REF05 and REF025 simulations. Salty and weakly stratified waters are found at around 42° S at the subsurface corresponding to the Subantarctic Mode waters (SAMW). The low salinity layer (34.2-34.4 psu) which appears at intermediate depth is typical of Antarctic Intermediate waters (AAIW) and can be traced back from the surface. A salty tongue (more than 34.7 psu) is found at around 2000 m depth and corresponds to Circumpolar Deep Water (CDW) which flows southward and upwells near the Polar Front. REF05 and REF025 simulations show very few differences: fronts are more localized in REF025; SAMW appears more northward in REF05 and are less salty than in REF025; AAIW downwells deeper and more southward in REF05 than in REF025. Simulated structures and values of salinity are generally in good agreement with the hydrography observed in this region (section I9 of the Southern Ocean WOCE hydrographic Atlas, Orsi and Whitworth (2004)), although AAIW and SAMW are slightly denser in the model.

Further validation, with respect to PERIANT05, is carried out in a companion paper (Zika et al. submitteda). For detailed validation of the global simulations ORCA05 and ORCA025, of which PERIANT05 and PERIANT025 are regional extractions, the reader is referred to Barnier et al. (2006) and Biastoch et al. (2008).

3. Southern Ocean dynamical response to changes in wind pattern and intensity

In what follows we present results from the series of experiments described in Section 2.b.

a. Response of the ACC transport

1) Shift of the ACC mean position

The Polar Front (PF) and Subantarctic Front (SAF) are the two main fronts which compose the ACC, since they can carry up to 75% of the total ACC transport south of Australia (Rintoul and Sokolov 2001). Monitoring the position of those fronts is then a good indicator of the ACC position. Here, we calculate the PF and SAF positions using a comparable method to that of Sallée et al. (2008), computing the surface dynamic height anomaly referenced to $1500m$. Following Sallée et al. (2008), the PF is defined by the $0.95m$ contour and the SAF by the $1.20m$ contour. Fig. 2 shows the mean PF and SAF positions for the period 1995-2004 for REF05 and SAM05+++ experiments and their corresponding experiments at 0.25°. Front positions as given by Orsi et al. (1995) are also shown. In REF05 and REF025, the PF and SAF mean positions as well as their meanders are in good agreement with the frontal descriptions proposed by Orsi et al. (1995). A closer look at the differences between the REF05 and REF025 experiments shows that, in the REF025 experiment, the ACC is much more spatially variable, making larger meanders and being in many places either narrower (at Drake Passage, Kerguelen Plateau) or wider (southeast Indian ocean, south Australia and southeast Pacific) than in the REF05 experiment (see also Table2). This is mostly due to both the more energetic mesoscale activity and a more precise resolution of the bathymetry in the REF025 experiment.

During positive phases of the SAM, it is found that fronts tend to shift poleward in the Atlantic and Indian basins and equatorward in the Pacific basin (Fig. 2). The response of the ACC mean position to positive SAM events is thus not zonally constant, due to

the pattern of SAM-driven wind anomalies. In addition, it can be noted that the frontal variability induced by SAM positive events is stronger in SAM025+++ experiment than in SAM05+++ experiment. However, in many regions, which correspond to major topographic features such as South-Atlantic mid-ocean ridge or Kerguelen Plateau, fronts show no spatial variability. WIND05+++ and WIND025+++ experiments show similar results, exhibiting large equatorward meanders downstream of the major topographic features and showing generally a stronger response than in the SAM forcing experiments (not shown).

Table 2 gives the ACC mean position over 1995-2004 computed from the averaging of PF and SAF mean positions over the same period. Increasing winds entails a narrowing of the ACC meaning a strengthening of the current. At 0.5°, it can be noted that SAM positive events induce a shift, either poleward or equatorward, of the ACC mean position of less than 0.5°. Considering the resolution, this shift cannot be considered significant and would rather be attributed to the turbulent nature of the ACC. Results from SAM025+++ though suggest a significant poleward shift of the ACC mean position of 0.3°. However, considering the turbulent nature of the ACC, more simulations at 0.25° would be needed to state if this poleward shift is systematic. At both 0.5°and 0.25°, intensifying winds homogeneously over the Southern Ocean induces a significant equatorward shift of the ACC mean position of more than 1°.

Hence, the response of the ACC mean position to SAM positive events is rather weak, despite the large increase in wind intensity and the shift of zonal winds by few degrees applied in our experiments. Moreover, it can also be noted that shifts of the ACC mean position found in our experiments are weaker than the poleward shifts of 1.0 ± 0.9^o found by Fyfe and Saenko (2006) and of 3.5^o found by Spence et al. (2010). Our results show that

the bathymetry is by far the main driver in setting the ACC pathway. However, downstream of major topographic features, fronts are much more sensitive to atmospheric forcing and become more spatially variable (Sallée et al. 2008). In those regions, SAM-driven wind anomaly patterns induce meridional shifts of fronts.

2) Acceleration of the ACC

Figure 5.a shows the time-averaged mass transport at Drake Passage over the last ten years of simulation (1995-2004) for each experiment as a function of the average zonal wind stress across the whole domain. The set of experiments shows a large range of responses of the ACC transport to winds. However, the strongest response is only a 12% increase in the ACC transport as shown in the SAM05+++ experiment.

Comparing ACC transport in the SAM05 and WIND05 experiments leads to two comments. Firstly, we can note linear relationships between the mean zonal wind stress and the mean ACC transport in the WIND05 and the SAM05 experiments, with a square linear correlation coefficient of more than 0.98 and of 0.93, respectively. This implies, as many studies have shown (e.g. Marshall and Radko 2003), that larger zonal wind stress leads to a larger ACC transport. Secondly, if we consider the respective slopes of those quasi-linear relationships, we can remark that the slope of the SAM05 series of experiments is far steeper than the one of the WIND05 series of experiments. This implies that the SAM forcing is far more efficient in accelerating the ACC than the WIND forcing. That is the poleward shift in the wind stress associated with the SAM acts to accelerate the ACC. The mechanism by which a poleward shift in the wind stress accelerates the ACC in run experiments is investi-

gated in Zika et al. (submitteda), who find that positive wind curl anomalies between Cape Horn and South Georgia Island, where the ACC flows equatorward over shallow topography, can cause positive anomalies in the total ACC transport. The poleward shift in the wind stress in the SAM forcing causes a positive wind curl anomaly near Cape Horn (by shifting the wind stress maximum to the South), while the WIND forcing causes a negative wind curl anomaly (by increasing the wind stress maximum positioned to the North). In any case, our experiments demonstrate that the spatial pattern, and not only the magnitude, of the wind stress, can play a major role in changing the ACC transport.

Comparing SAM05+++ to SAM025+++, we see that at finer resolution resolving eddies attenuates the response of the ACC to poleward intensified winds by 5%. This result, held in isolation, is in good agreement with many other modeling studies which have suggested that the response of the ACC to increased wind forcing might be reduced as resolution is increased (Hallberg and Gnanadesikan 2006; Spence et al. 2010; Farneti et al. 2010). This is by no means a general finding. Comparing WIND05+++ to WIND025+++, we see that with finer resolution the ACC transport is increased. This is in disagreement with the findings of Hallberg and Gnanadesikan (2006) and cast doubt on the idea that at finer and finer resolution the simulations of the ACC will necesseraly converge towards an eddy saturated regime (Hogg et al. 2008).

b. Response of the meridional overturning circulation

It is appropriate to consider the MOC in potential density, rather than in depth space. Following Döös and Webb (1994), the total meridional overturning streamfunction, Ψ_{tot} can

be expressed as:

$$\Psi_{tot}(y,\sigma_2) = \overline{\oint \int_{-H}^{\tilde{z}(x,y,\sigma_2)} v \, d\tilde{z}' \, dx} \tag{3}$$

where σ_2 is the 2000m depth referenced potential density, H the spatially varying ocean depth, and $\tilde{z}$ the depth of the isopycnal σ_2. The overbar denotes a temporal average at constant depth. That is, for some variable ξ over some period τ, $\overline{\xi} = \int_0^\tau \xi dt/\tau$. Then, the transient eddy-induced circulation Ψ^*, i.e. that due to deviations from the temporal mean, is defined following Treguier et al. (2007) as:

$$\begin{cases} \overline{\Psi}(y,\sigma_2) = \oint \int_{-H}^{\overline{\tilde{z}(x,y,\sigma_2)}} \overline{v} d\overline{\tilde{z}'} dx, \\ \Psi^* = \Psi_{tot} - \overline{\Psi} \end{cases} \tag{4}$$

where $\overline{\Psi}$ is the mean Eulerian circulation computed from the time-mean velocity and the time-mean potential density field.

Fig.6 shows the total meridional overturning computed from 5-day-averaged outputs from the simulations, and its Eulerian and transient-eddy contributions for each experiment during the 1995-2004 period. Considering the total meridional overturning (Fig.6, left panels), the strong uppermost blue cell which extends from the north of the domain to roughly 40°S corresponds to the wind-driven *subtropical cell* which bring light waters to the south and, as they become colder, transform into SAMW. The red cell which extends until 57°S corresponds to the *subpolar cell* where North Atlantic Deep Waters (NADW) coming from the north, are brought to the surface at 57°S by Ekman pumping, transform into AAIW by surface fluxes and flow back to the north. Below this, the blue cell corresponds to the *deep cell* where Circumpolar Deep Waters (CDW) upwell farther south, transform into AABW by a fresh water input and downwell back to the north along continental slopes. Finally, the upper blue cell which extends from 45°S to 65°S is the expression of waters getting colder,

so denser, as they go southward while flowing along the ACC. This is not seen if the MOC is computed along streamlines rather than latitude lines (Treguier et al. 2007; Zika et al. submittedb). This upper cell does, however, constitute a genuine overturning in density space. The Eulerian overturning (Fig.6, middle panels) shows the same general structure as the total overturning. This Eulerian overturning is partly compensated by the transient-eddy overturning (Fig.6, right panels) as described by equation (4).

The subtropical, subpolar and deep cells of the total overturning are rather similar in REF05 and REF025 experiments, each cell roughly transporting up to $\sim 15\ Sv$, $\sim 8\ Sv$ and $\sim 10\ Sv$, respectively. While intensities of both subtropical and subpolar cells of the Eulerian overturning are very similar in REF05 and REF025 experiments, the upper cell linked to the ACC pathway shows a weak intensification of up to $\sim -5\ Sv$ in REF025. So does the transient-eddy cell. Such a response is expected, since higher resolution leads to better-resolved turbulence and bathymetry.

1) Modification of the MOC density structure

Fig. 6 shows a net poleward shift of the southernmost extent of the subpolar cell in the total overturning by roughly 4° in the SAM025+++ experiment. It is comparable - even if larger - to what Farneti et al. (2010) found in their CM2.4 model. We can note, moreover, that such a shift is not observed in the SAM05+++ experiment. This result is related to the significant, albeit weak, poleward shift found in the ACC mean position in the SAM025+++ experiment only (see Section 3.1). Concomitantly, the subpolar cell is found to transform deep waters into comparatively (i) denser waters in the SAM experiments than in the REF

experiments (from $\sim 35.7\ kg.m^{-3}$ to $\sim 35.9\ kg.m^{-3}$) and (ii) far lighter waters in the WIND experiments than in the REF experiments (from $\sim 35.7\ kg.m^{-3}$ to $\sim 35.4\ kg.m^{-3}$). This result is consistent with what Hallberg and Gnanadesikan (2006) found in their study. The subptropical cell transforms comparatively denser waters in the SAM experiments than in the REF and WIND experiments (from $\sim 35.2\ kg.m^{-3}$ to $\sim 35.8\ kg.m^{-3}$). This result is also observed by Oke and England (2004) who diagnose a cooling of SAMW consequent to a poleward shift of zonal winds.

Indeed, an anomalous intensification of zonal winds over the ACC latitudes leads to a change in wind curl and as a consequence a change in the location of the Ekman divergence. The deep waters coming from the north are thus expected to upwell more poleward where, while interacting with a colder atmosphere, they give up more heat and transform into comparatively denser water masses. However, when the wind is homogeneously increased over the Southern Ocean, as occurs in the WIND experiments, ACC fronts shift equatorward, so that intermediate waters downwell more equatorward along comparatively lighter isopycnal surfaces.

Therefore, SAM positive events can indeed imply significant changes in water masses properties which in turn, will impact their rate of formation (Oke and England 2004; Sen Gupta and England 2006; Hallberg and Gnanadesikan 2006). Those results also point out that the MOC density structure responds in a very different way to homogeneous wind anomalies than to SAM-induced wind anomalies.

2) Intensification of the subpolar MOC

The evolution of the Southern Ocean carbon sink has been shown to be mainly driven by SAM-induced intensification of the MOC, resulting in higher levels of DIC concentration at the surface (Lenton and Matear 2007; Lovenduski et al. 2007, 2008). The upwelling of DIC-rich water masses is part of the circulation described by the subpolar cell. In what follows, we thus focus on the response of the subpolar cell to wind anomalies.

To this, an estimation of the subpolar MOC intensity is computed by calculating the maximum of Ψ_{tot} in the subpolar overturning between 40°S and 55°S. Figure 5.b shows this estimation over the last ten years of simulation (1995-2004) for each experiment as a function of the mean zonal wind stress over the model domain. The set of experiments shows a large range of responses of the subpolar MOC to winds, the strongest response being a 153% increase in the subpolar MOC in the WIND05+++ experiment. In fact, the subpolar MOC seems to be much more sensitive to changes in winds in our model than in other modeling studies (Hallberg and Gnanadesikan 2006; Farneti et al. 2010).

Comparing the response of the subpolar MOC intensity in the SAM05 and WIND05 experiments leads to two comments. Firstly, we can note a linear relationships between the mean zonal wind stress and the mean subpolar MOC intensity, with a square linear correlation coefficient of more than 0.99 and of 0.91, respectively. This tends to show, as already discussed in many previous studies (Gnanadesikan and Hallberg 2000; Karsten et al. 2002), that the wind sets the MOC intensity at first order. Secondly, if we consider the respective slopes of those quasi-linear relationships, we can remark that the slope of the WIND05 series of experiments is slightly steeper than the one of the SAM05 series

of experiments. This implies that the WIND forcing is more efficient in intensifying the subpolar MOC than the SAM forcing. Indeed, in the WIND forcing, the wind stress is increased over a greater range of latitudes. This implies that the Ekman pumping anomaly to the north and south of the ACC are spread out over a greater number of latitudes in the WIND05 experiments, perhaps leading to a more robust change in the subpolar MOC.

Fig. 5.b also shows that better resolving eddies attenuates the response of the subpolar MOC to a homogeneous wind anomaly but enhances the subpolar MOC response to a SAM-induced wind anomaly. However, as mesoscale activity is better resolved, the response of the subpolar MOC to increased wind stress is expected to be attenuated. This is in particular reported by Hallberg and Gnanadesikan (2006) and Farneti et al. (2010), who argue that this attenuation is caused transient eddy fluxes which better compensate for the increased Ekman transport in the MOC. In fact, in the SAM025+++ experiment, the role of transient eddies in the meridional overturning reduces and becomes almost non-existent (bottom right panel of Fig.6). This result suggests that a process other than meridional transient eddy fluxes contributes to meridional fluxes and act in compensating for the large increase in zonal Ekman transport. This is discussed in the following section.

4. Discussion

As introduced in equation (4), the total circulation Ψ_{tot} can be decomposed into a mean Eulerian circulation $\overline{\Psi}$ and a transient eddy-induced circulation Ψ^*. $\overline{\Psi}$ accounts for the temporal mean flow and thus holds the contribution of the zonally averaged flow, that is mainly the Ekman transport, and the meridional excursions from the zonal mean, that is the

standing eddies. In the same way that the temporal mean and transient eddy (perturbation) components of the MOC can be separated, as can the zonally averaged and standing eddy components such that:

$$\begin{cases} \overline{\Psi} = < \overline{\Psi} > + \overline{\Psi_{SE}} \\ < \overline{\Psi} > (y, \sigma_2) = \oint \int_{-H}^{<\overline{\tilde{z}(y,\sigma_2)}>} < \overline{v} > \, d < \overline{\tilde{z}'} > dx, \end{cases} \tag{5}$$

where the angular brackets denote a zonal average at constant depth. That is, for some function ξ and latitude circle of length L, $< \xi >= \oint \xi dx/L$. The streamfunction $< \overline{\Psi} >$ is effectively the Eulerian mean MOC zonally averaged at constant depth and projected onto the zonally averaged density. At latitudes of Drake Passage, $< \overline{\Psi} >$ largely corresponds to a northward Ekman transport on shallow layers and a southward geostrophic transport on layers whose mean depth is below the Drake Passage. The streamfunction $\overline{\Psi_{SE}}$ accounts for the standing eddy overturning circulation. Thus, the total circulation can be defined in terms of three main contributions, as follows:

$$\Psi_{tot} = < \overline{\Psi} > + \overline{\Psi_{SE}} + \Psi^* \tag{6}$$

Fig. 7 shows the Eulerian mean circulation zonally averaged $< \overline{\Psi} >$ and the standing eddy-driven circulation $\overline{\Psi_{SE}}$ for SAM05+++ and SAM025+++ experiments during the 1995-2004 period. This figure shows in both experiments that $< \overline{\Psi} >$ is partly compensated by $\overline{\Psi_{SE}}$. At higher resolution, it is found that the standing eddy-driven circulation is reinforced. As in Section 2, we define an index of the MOC intensity for $< \overline{\Psi} >$ (resp. $\overline{\Psi_{SE}}$) based on the maximum of $< \overline{\Psi} >$ (resp. $\overline{\Psi_{SE}}$) in the overturning between 40°S and 55°S. Using those indexes, it is found that the relative contribution of the standing eddy-driven circulation ($\overline{\Psi_{SE}}$) to the Eulerian mean circulation zonally averaged ($< \overline{\Psi} >$) is increased by

more than 10% between SAM05+++ and SAM025+++ experiments (see also Fig. 7). That is, at higher resolution, standing eddy-driven transport better compensates for the increase in the Ekman transport. This result is also consistent with the respective responses of the WIND05+++ and WIND025+++ experiments (not shown).

This study finds that at higher resolution, transient eddy fluxes can be weakened in the meridional direction and that standing eddy meridional fluxes can be invigorated. The majority of the overturning circulation being a balance of Ekman transport and the time-mean geostrophic flow. An enhancement of the standing eddy meridional overturning, instead of the transient eddy meridional overturning, is perhaps not unexpected in light of previous studies. Consider Farneti et al. (2010) for example. There, two fine resolution experiments are subjected to present day and SAM-like forcing anomalies (their CTL and SHW3X experiments, respectively). The SAM-like anomalies involve amplification of the northward Ekman transport of around 20 Sv at Drake Passage latitudes (their Fig.4c) with little change in the density space meridional overturning. The eddy driven overturning response is only 2-3 Sv (their Fig.10). Clearly, the standing eddy meridional overturning compensates for the majority of the 20 Sv change in Ekman transport.

Changes in standing eddy meridional fluxes are due both to enhanced deviations from the zonal mean of velocity ($v- < v >$) and enhanced deviations in the zonal mean of isopycnal thickness ($h- < h >$, where $h = \frac{d\tilde{z}}{d\sigma_2}$), that is the stratification. Higher resolution implies more turbulence as well as finer topography, thus allowing more standing eddy features to exist (see Fig.2), and to be more vigorous, that is changing $v- < v >$. At the same time, changes in the resolution can cause large scale changes in stratification, perhaps in part caused by transient eddies.

The shut down in the transient eddy component of the subpolar meridional overturning in the SAM025+++ experiment, comes despite an increase in EKE and an attenuation in the response of the ACC while getting to higher resolution. This suggests an active transient eddy field in SAM025+++. In fact, a recent study by Zika et al. (submittedb) demonstrates the key role of transient eddies in the overturning circulation of the Southern Ocean. They find, using a similar modelling system to ours, that while the mean flow is largely responsible for compeating the Ekman transport *meridionally*, transient eddies compensate *vertically*. The mean flow transports light water southward creating zonal density gradients. Transient eddies then act on those gradients, fluxing light water upward.

5. Conclusion

Simulations of the Southern Ocean using an ocean-sea ice model forced by the atmosphere have been run at two eddy-permitting to eddy resolving resolutions (0.5° and 0.25°) for 25 years (1980-2004). In order to investigate the ACC and MOC responses to SAM pattern and intensity, two types of synthetic forcing are applied: the WIND forcing where winds are increased over the Southern Ocean, and the SAM forcing where a wind anomaly corresponding to a SAM positive phase is added to the original forcing.

During positive phases of the SAM, it is found that the ACC is accelerated by roughly 10% and poleward shifted by less than 0.5°, as a result of a stronger wind stress and a modified wind curl. The subpolar MOC is largely intensified by the increased wind stress which confirms that the overturning circulation is set at first order by the wind-driven circulation. Moreover, significant changes occur in the MOC density structure: the subpolar

cell is shifted poleward by roughly 4° while the overturning draws on denser intermediate waters.

Moreover, it is found that standing eddy fluxes more efficiently balance the Ekman flow as resolution increases and that meridional transient eddy fluxes may not be enhanced while increasing winds and resolution. In one case, standing eddies account alone in the meridional fluxes that act to compensate for the wind-driven circulation. This particular case underlines the crucial role played by standing eddies in the meridional overturning of the Southern Ocean.

Moreover, it appears that the response of the MOC intensity to changes in winds cannot be directly inferred from the response of the ACC transport. Although MOC and ACC transport are driven by the same dynamical processes, those processes do not set at the same order the respective balances of the MOC and ACC transports.

Finally, modifying the pattern of wind anomalies leads to different responses of the ACC and MOC. The pattern of SAM-driven wind anomalies is found to be far more efficient at accelerating the ACC. This shows that experiments which aim to simulate the response of the Southern Ocean to the SAM must take into account the spatial modulation of wind anomalies. It is also important that the SAM pattern simulated by the coupled climate models, such as the ones used by the IPCC, be assessed.

Acknowledgments.

We would like to thank J.M. Molines for his modelling support. For this project, C.O. Dufour and M. Gehlen are supported by the French CEA (Commissariat à l'Energie Atom-

ique). J. Le Sommer and B. Barnier are supported by the French CNRS (Centre National de la Recherche Scientifique). J.D. Zika is supported by the Agence Nationale de la Recherche through contract ANR-08-JCJC-0777-01. Simulations were carried out at the CNRS IDRIS super computer facility in Orsay France and at the CINES super computer facility in Montpellier, France.

APPENDIX

3D thermohaline restoring of AABW

Thermohaline properties of Antarctic Bottom Waters (AABW) are restored towards the climatology of Gouretski and Koltermann (2004) using the following method.

Following Orsi et al. (1999), in the Southern Ocean, AABW are generally defined where $\sigma_2 > 37.11\ kg.m^{-3}$, σ_2 being the potential density referenced at 2000m depth. Based on this density criterion, a mask (M) of the domain is built as follows:

$$M(x,y,z) = g(\sigma_2(x,y,z)) \cdot h(z) \tag{A1}$$

$$with \begin{cases} g(\sigma_2(x,y,z)) = \frac{1}{2}[\frac{tanh[(\sigma_2(x,y,z)-\sigma_{ref}]}{\alpha} + 1] \\ h(z) = \frac{1}{2}[\frac{tanh[(z-z_{ref}]}{\beta} + 1] \end{cases} \tag{A2}$$

where σ_2 is computed from the annual climatology of Gouretski and Koltermann (2004), $\sigma_{ref} = 37.16\ kg.m^{-3}$, $\alpha = 0.025\ kg.m^{-3}$, $z_{ref} = 1000m$ and $\beta = 100m$. M thus holds values ranging from 0 to 1.

On the one hand, the NODC (Levitus) World Ocean Atlas 1998 is used both to initialize the temperature and salinity fields and apply the restoring in our simulations, because it is a monthly climatology. On the other hand, the annual climatology of Gouretski and Koltermann (2004) is chosen to build the AABW restoring mask because the interpolation method used to compute this climatology keeps it from creating spurious water masses as it appears in the NODC (Levitus) World Ocean Atlas 1998.

Along the whole simulation, thermohaline properties computed by the model are restored towards the NODC (Levitus) World Ocean Atlas 1998, as follows:

$$\begin{cases} \Theta(t,x,y,z) = \Theta(t,x,y,z) + \frac{M(x,y,z)}{\tau}(\Theta_{clim}(x,y,z) - \Theta(t,x,y,z)) \\ S(x,y,z) = S(t,x,y,z) + \frac{M(x,y,z)}{\tau}(S_{clim}(x,y,z) - S(t,x,y,z)) \end{cases} \tag{A3}$$

where, Θ and S are potential temperature and salinity computed by the model, respectively; Θ_{clim} and S_{clim} potential temperature and salinity from the NODC (Levitus) World Ocean Atlas 1998, respectively; and τ the restoring time scale.

Fig.8 shows the ratio of water depth restored with a time scale of less than ten years in the simulations performed. That is to say a total restoring coefficient $\frac{M(x,y,z)}{\tau} > 3,17.10^{-9}\ s^{-1}$, corresponding to a mask coefficient $M(x,y,z) > 0.2$ and a restoring time scale $\tau = 2\ years$. The constraint on the model is strongest around the Antarctic mainland and becomes gradually weaker as we go northward. This is due to the presence of very dense water masses which form on the Antarctic ice shelves and then spread along continental slopes. However, it is worth noting that the restoring is quite weak on the latitude band corresponding to the ACC.

The efficiency of the above method was tested in regional simulations of the Southern Ocean over the period 1991 to 2000 using the same modelling system (see Section 2 for details on the model and the configuration used). A series of sensitivity experiments to the potential density criterion σ_{ref} (determining the amount of water masses restored) on the one hand, and the restoring time scale τ on the other hand, was carried out. All the sensitivity experiments showed a shortened spin-up compared to the reference experiment, with an ACC transport stabilizing after few years of simulation (see Fig.3). After the spin-up, no more trend appeared in the ACC transport in the sensitivity experiments contrary to the

reference experiment. Moreover, the interannual variability of the ACC transport was found insensitive to the restoring of bottom waters. Finally, the bigger the restoring constraint on AABW was, the more intense the ACC transport was. σ_{ref} and τ criteria were thus chosen to give a reasonably good intensity of the ACC transport while setting the lowest constraint on the model as possible. A similar method was also used by Hallberg and Gnanadesikan (2006) who applied weak sponges around the Antarctic ice shelves to ensure the formation of Antarctic Bottom Water. These authors also noticed that this restoring influenced the net transport of the ACC.

REFERENCES

Barnier, B., et al., 2006: Impact of partial steps and momentum advection schemes in a global ocean circulation model at eddy permitting resolution. *Oc. Dynam.*, **4**, DOI 10.1007/s10 236–006–0082–1.

Biastoch, A., C. Böning, J. Getzlaff, J. Molines, and G. Madec, 2008: Causes of Interannual-Decadal Variability in the Meridional Overturning Circulation of the Midlatitude North Atlantic Ocean. *J. Climate*, **21**, 6599–6615.

Böning, C., A. Dispert, M. Visbeck, S. Rintoul, and F. Schwarzkopf, 2008: The response of the Antarctic Circumpolar Current to recent climate change. *Nature Geoscience*.

Brodeau, L., B. Barnier, T. Penduff, A.-M. Treguier, S. Gulev, and T. J. McDougall, 2010: An ERA-40 based atmospheric forcing for global ocean circulation models. *Oc. Modell.*, **31**, 88–104.

Cai, W. and P. H. Whetton, 2003: The Response of the Antarctic Oscillation to Increasing and Stabilized Atmospheric CO_2. *J. Climate*, **16**, 1525–1538.

Cunningham, S. A., S. G. Alderson, B. A. King, and M. A. Brandon, 2003: Transport and variability of the Antarctic Circumpolar Current in Drake Passage. *J. Geophys. Res.*, **108**, NO. C5, 8084.

Döös, K. and D. J. Webb, 1994: The Deacon Cell and the Other Meridional Cells of the Southern Ocean. *J. Phys. Oceanogr.*, **24**, 429–442.

Drakkar Group, 2007: Eddy-permitting Ocean Circulation Hindcasts of past decades. *CLIVAR Exchanges*, **12**, 8–10.

Farneti, R., T. L. Delworth, A. J. Rosati, S. M. Griffies, and F. Zeng, 2010: The role of mesoscale eddies in the rectification of the southern ocean response to climate change. *J. Phys. Oceanogr.*, **40**, 1539–1557.

Fichefet, T. and M. A. M. Maqueda, 1997: Sensitivity of a global sea ice model to the treatment of ice thermodynamics and dynamics. *J. Geophys. Res.*, **102**.

Fyfe, J. C. and O. A. Saenko, 2006: Simulated changes in the extratropical Southern Hemisphere winds and currents. *Geophys. Res. Letters*, **33**, L06 701.

Gent, P. R. and J. C. McWilliams, 1990: Isopycnal Mixing in Ocean Circulation Models. *J. Phys. Oceanogr.*, **20**, 150–155.

Gnanadesikan, A. and R. W. Hallberg, 2000: On the Relationship of the Circumpolar Current to Southern Hemisphere Winds in Coarse-Resolution Ocean Models. *J. Phys. Oceanogr.*, **30**, 2013–2034.

Gouretski, V. and K. Koltermann, 2004: Woce global hydrographic climatology, a technical report. *Berichte des BSH*, **35**.

Hall, A. and M. Visbeck, 2002: Synchronous Variability in the Southern Hemisphere Atmosphere, Sea Ice, and Ocean Resulting from the Annular Mode. *J. Climate*, **15**, 3043–3057.

Hallberg, R. and A. Gnanadesikan, 2006: The Role of Eddies in Determining the Structure and Response of the Wind-Driven Southern Hemisphere Overturning: Results from the

Modeling Eddies in the Southern Ocean (MESO) Project. *J. Phys. Oceanogr.*, **36**, 2232–2252.

Hogg, A. M., 2010: An Antarctic Circumpolar Current driven by surface buoyancy forcing. *Geophys. Res. Lett.*

Hogg, A. M., M. P. Meredith, J. R. Blundell, and C. Wilson, 2008: Eddy Heat Flux in the Southern Ocean: Response to Variable Wind Forcing. *J. Climate*, **21**, 608–620.

Karsten, R., H. Jones, and J. Marshall, 2002: The Role of Eddy Transfer in Setting the Stratification and Transport of a Circumpolar Current. *J. Phys. Oceanogr.*, **32**, 39–54.

Klinger, B. A. and C. Cruz, 2009: Decadal response of global circulation to southern ocean zonal wind stress perturbation. *J. Phys. Oceanogr.*, **39**, 1888–1904.

Le Quéré, C., et al., 2007: Saturation of the southern ocean CO_2 sink due to recent climate change. *Science*, **316**, 1735.

Lee, M.-M., A. C. Coward, and A. J. G. Nurser, 2002: Spurious diapycnal mixing of the deep waters in an eddy-permitting global ocean model. *J. Phys. Oceanogr.*, **32**, 1522–1535.

Lefebvre, W. and H. Goose, 2005: Influence of the Southern Annular Mode on the sea ice-ocean system: the role of the thermal and mechanical forcing. *Oc. Science*, **1**, 145–157.

Lenton, A. and R. J. Matear, 2007: Role of the southern annular mode (sam) in southern ocean CO_2 uptake. *Global Biogeochem. Cycles*, **21**.

Lombard, A., G. Garric, and T. Penduff, 2009: Regional patterns of observed sea level

change: Insights from a 1/4°global ocean/sea-ice hindcast. *Oc. Dynamics*, **59(3)**, 433–449.

Lovenduski, N., N. Gruber, and S. Doney, 2008: Toward a mechanistic understanding of the decadal trends in the Southern Ocean carbon sink. *Global Biogeochem. Cycles*, **22**, GB3016.

Lovenduski, N., N. Gruber, S. Doney, and I. Lima, 2007: Enhanced CO2 outgassing in the Southern Ocean from a positive phase of the Southern Annular Mode. *Global Biogeochem. Cycles*, **21**, GB2026.

Madec, G., 2008: Nemo ocean engine. *Note du Pôle de modelisation, Institut Pierre-Simon Laplace (IPSL), France*, **27**, ISSN 1288–1619.

Madec, G., P. Delecluse, M. Imbard, and C. Lévy, 1999: OPA8.1 Ocean General Circulation Model reference manual. *Note du Pôle de modelisation, Institut Pierre-Simon Laplace (IPSL), France*, 91 pp.

Marshall, G. J., 2003: Trends in the Southern Annular Mode from Observations and Reanalyses. *J. Climate*, **16**, 4134–4143.

Marshall, G. J., P. A. Stott, J. Turner, W. M. Connolley, J. C. King, and T. A. Lachlan-Cope, 2004: Causes of exceptional atmospheric circulation changes in the Southern Hemisphere. *Geophys. Res. Lett.*, **31**.

Marshall, J. and T. Radko, 2003: Residual-mean solutions for the antarctic circumpolar current and its associated overturning circulation. *J. Phys. Oceanogr.*, **33**, 2341–2354.

Meredith, M. P. and A. M. Hogg, 2006: Circumpolar response of Southern Ocean eddy actvity to a change in the Southern Annular Mode. *Geophys. Res. Lett.*, **33**.

Metzl, N., B. Tilbrook, and A. Poisson, 1999: The annual fCO_2 cycle and the air-sea CO_2 flux in the sub-Antarctic Ocean. *Tellus*, **51**.

Oke, P. R. and M. R. England, 2004: Oceanic Response to Changes in the Latitude of the Southern Hemisphere Subpolar Westerly Winds. *J. Climate*, **17**, 1040–1054.

Orsi, A., T. W. III, and J. W. Nowlin, 1995: On the meridional extent and fronts of the Antarctic Circumpolar Current. *Deep Sea Res., Part II*, **42**, 641–673.

Orsi, A., G. Johnson, and J. Bullister, 1999: Circulation, mixing, and roduction of Antarctic Bottom Water. *Progress in Oceanography*, **43**, 55–109.

Orsi, A. and T. Whitworth, 2004: Hydrographic Atlas of the World Ocean Circulation Experiment (WOCE). Volume 1 : Southern Ocean. *International WOCE Project Office, Southampton, U.K.*

Renner, A., K. Heywood, and S. Thorpe, 2009: Validation of three global ocean models in the Weddell Sea. *Oc. Modelling*, **30**, 1–15.

Rintoul, S. and S. Sokolov, 2001: Baroclinic transport variability of the Antarctic Circumpolar Current south of Australia (WOCE repeat section SR3). *J. Geophys. Res.*, **106**, 2795–2814.

Sallée, J.-B., K. Speer, and R. Morrow, 2008: Response of the Antarctic Circumpolar Current to Atmospheric Variability. *J. Climate*, **21**, 3020–3039.

Sen Gupta, A. and M. H. England, 2006: Coupled Ocean-Atmosphere-Ice Response to Variations in the Southern Annular Mode. *J. Climate*, **19**, 4457–4486.

Spence, P., J. C. Fyfe, A. Montenegro, and A. J. Weaver, 2010: Southern Ocean response to strenghening winds in an eddy-permitting global climate model. *J. Climate*.

Straub, D. N., 1993: On the transport and angular momentum balance of channel models of the Antarctic Circumpolar Current. *J. Phys. Oceanogr.*, **23**, 776–782.

Thompson, D. W. J. and S. Solomon, 2002: Interpretation of recent Southern Hemisphere climate change. *Science*, **296**, 895–899.

Thompson, D. W. J., J. M. Wallace, and G. C. Hegerl, 2000: Annular Modes in the Extratropical Circulation. Part II: Trends*. *J. Climate*, **13**, 1018–1036.

Treguier, A., J. L. Sommer, J. Molines, and B. D. Cuevas, 2010: Response of the Southern Ocean to the Southern Annular Mode: interannual variability and multidecadal trend.

Treguier, A.-M., B. Barnier, A. D. Miranda, J. Molines, N. Grima, M. Imbard, G. Madec, and C. Messager, 2001: An eddy-permitting model of the Atlantic circulation: Evaluating open boundary conditions. *J. Geophys. Res. - Oceans*, **106**.

Treguier, A.-M., M. H. England, S. R. Rintoul, G. Madec, J. Le Sommer, and J.-M. Molines, 2007: Southern Ocean overturning across streamlines in an eddying simulation of the Antarctic Circumpolar Current. *Oc. Science*, **3**, 491–507.

Whitworth, T., 1983: Monitoring the Transport of the Antarctic Circumpolar Current at Drake Passage. *J. Phys. Oceanogr.*, **13**.

Whitworth, T. and R. Peterson, 1985: Volume transport of the Antarctic Circumpolar Current from bottom pressure measurements. *J. Phys. Oceanogr.*, **15**.

Winton, M., R. Hallberg, and A. Gnanadesikan, 1998: Simulation of Density-Driven Frictional Downslope Flow in Z-Coordinate Ocean Models. *J. Phys. Oceanogr.*, **28**, 2163–2174.

Yang, X., R. Huang, J. Wang, and D. Wang, 2008: Delayed baroclinic response of the Antarctic circumpolar current to surface wind stress. *Science in Chine Series D: Earth Sciences*, **51**.

Zika, J. D., J. Le Sommer, and C. O. Dufour, submitteda: Localized Acceleration of the Antarctic Circumpolar Current. *J. Phys. Oceanogr.*

Zika, J. D., et al., submittedb: Destruction of the Deacon Cell by Vertical Eddy Fluxes. *Geophys. Res. Lett.*

List of Figures

1 (a) Regression pattern (arbitrary units) of 1980-2001 monthly averaged ERA-40 zonal winds onto the 1980-2001 monthly SAM index. Contours range from -1.4 to 1.4 with an intervall of 0.2. Continuous contour correspond to positive values and dashed contours to negative values. The SAM index comes from NCEP products. (b) 1995-2004 mean zonal wind stress (N/m^2) for the 0.5° series of experiments: REF05 simulation (solid line), WIND05+, WIND05++ and WIND05+++ simulations (dashed lines) and SAM05+, SAM05++ ans SAM05+++ simulations (dotted lines). 38

2 1992-2002 mean EKE in $(cm/s)^2$ (a-d) at 10 m depth the simulations and (e) from TOPEX-POSEIDON satellite data. Satellite data have been regrided to 0.25° resolution for comparison. Mean PF and SAF positions (a-d) for 1995-2004 computed in simulations following Sallée et al. (2008) and (e) from Orsi et al. (1995). (b,d): Black contours correspond to front locations in REF05 (resp. REF025) and red contours to front locations in SAM05+++ (resp. SAM025+++). 39

3 Time series of annual mass transport at Drake Passage (in Sv) for the DRAKKAR global simulation at 0.5° (grey solid line), the DRAKKAR global simulation at 0.25° (black solid line), the regional reference simulation at 0.5° (dash grey line) and the regional reference simulation at 0.25° (balck dashed line). . . . 40

4 Mean salinity (1995-2004) along the 115°E cross-section in the REF05 simulation (top panel) and the REF025 simulation (bottom panel) with a zoom on the upper 1000 m. Solid black contours indicate some surface referenced isopycnals. The colorbar indicates salinity in psu units. 41

5 (a) 1995-2004 mean mass transport at Drake Passage (in Sv) and (b) maximum of the 1995-2004 subpolar cell between 40°S and 55°S (in Sv) plotted against 1995-2004 mean zonal wind stress in $N.m^{-2}$, for REF simulations (circles), WIND simulations (triangles) and SAM simulations (squares). 0.5° simulations are in black and 0.25° simulations are in grey. 42

6 MOC (in Sv) in σ_2 potential density coordinates: (left) the total circulation Ψ_{tot}, (middle) the Eulerian-mean circulation $\overline{\Psi}$ and (right) the transient eddy-induced circulation Ψ^* for (from top to bottom) REF05, WIND05+++, SAM05+++, REF025, WIND025+++ and SAM025+++ experiments. Red cells correspond to clock-wise flows and blue cells to counter-clockwise flows. 43

7 MOC (in Sv) in σ_2 potential density coordinates: (left) the Eulerian mean circulation zonally averaged $< \overline{\Psi} >$, (right) the standing eddy-driven circulation $\overline{\Psi_{SE}}$ for (from top to bottom) SAM05+++ and SAM025+++ experiments. Red cells correspond to clock-wise flows and blue cells to counter-clockwise flows. 44

8 Percentage of the water depth restored with a time scale of less than ten years. That is to say a total restoring coefficient $\frac{M(x,y,z)}{\tau} > 3,17.10^{-9}\ s^{-1}$, corresponding to a mask coefficient $M(x,y,z) > 0.2$ and a restoring time scale $\tau = 2\ years$. 45

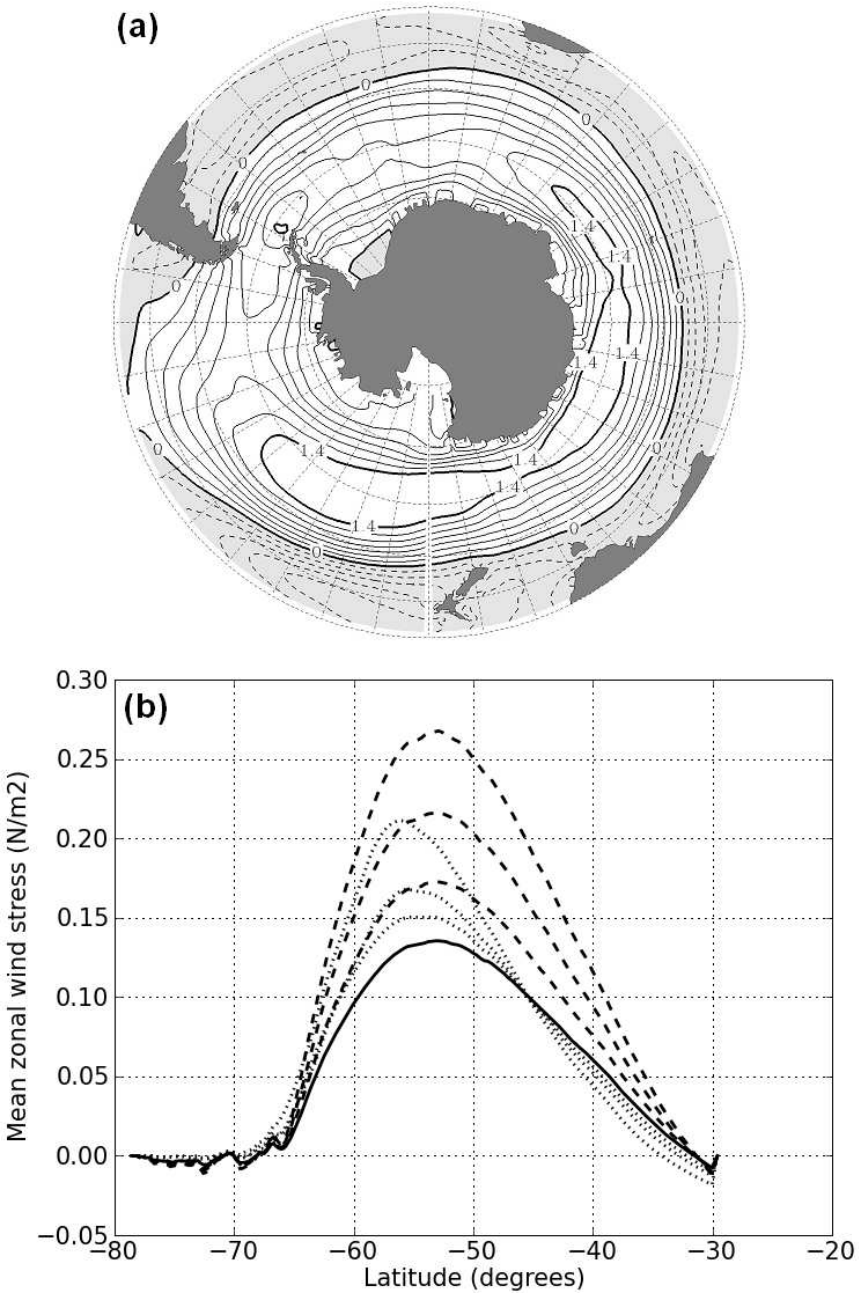

FIG. 1. (a) Regression pattern (arbitrary units) of 1980-2001 monthly averaged ERA-40 zonal winds onto the 1980-2001 monthly SAM index. Contours range from -1.4 to 1.4 with an intervall of 0.2. Continuous contour correspond to positive values and dashed contours to negative values. The SAM index comes from NCEP products. (b) 1995-2004 mean zonal wind stress (N/m^2) for the 0.5° series of experiments: REF05 simulation (solid line), WIND05+, WIND05++ and WIND05+++ simulations (dashed lines) and SAM05+, SAM05++ ans SAM05+++ simulations (dotted lines).

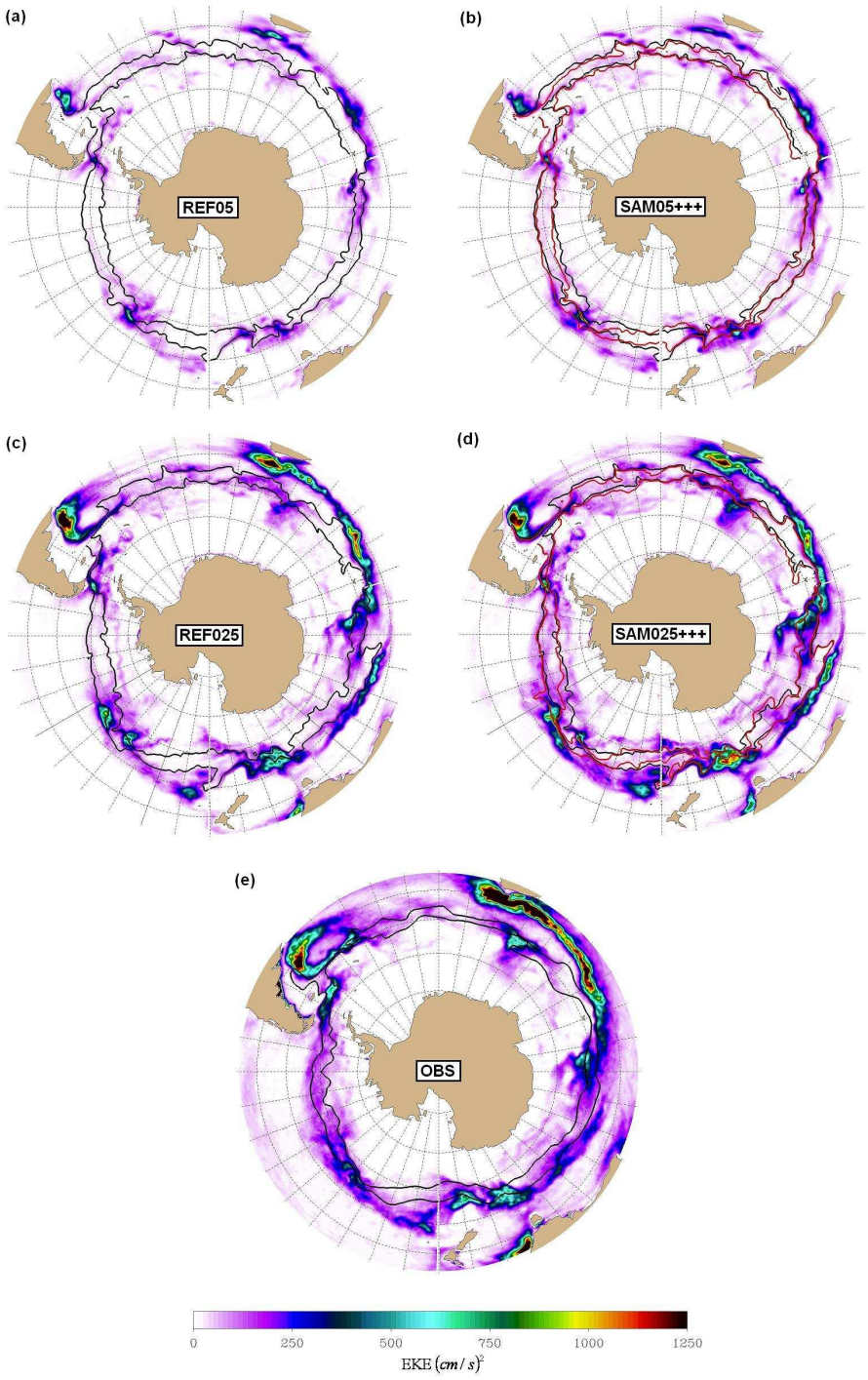

FIG. 2. 1992-2002 mean EKE in $(cm/s)^2$ (a-d) at 10 m depth the simulations and (e) from TOPEX-POSEIDON satellite data. Satellite data have been regrided to 0.25° resolution for comparison. Mean PF and SAF positions (a-d) for 1995-2004 computed in simulations following Sallée et al. (2008) and (e) from Orsi et al. (1995). (b,d): Black contours correspond to front locations in REF05 (resp. REF025) and red contours to front locations in SAM05+++ (resp. SAM025+++).

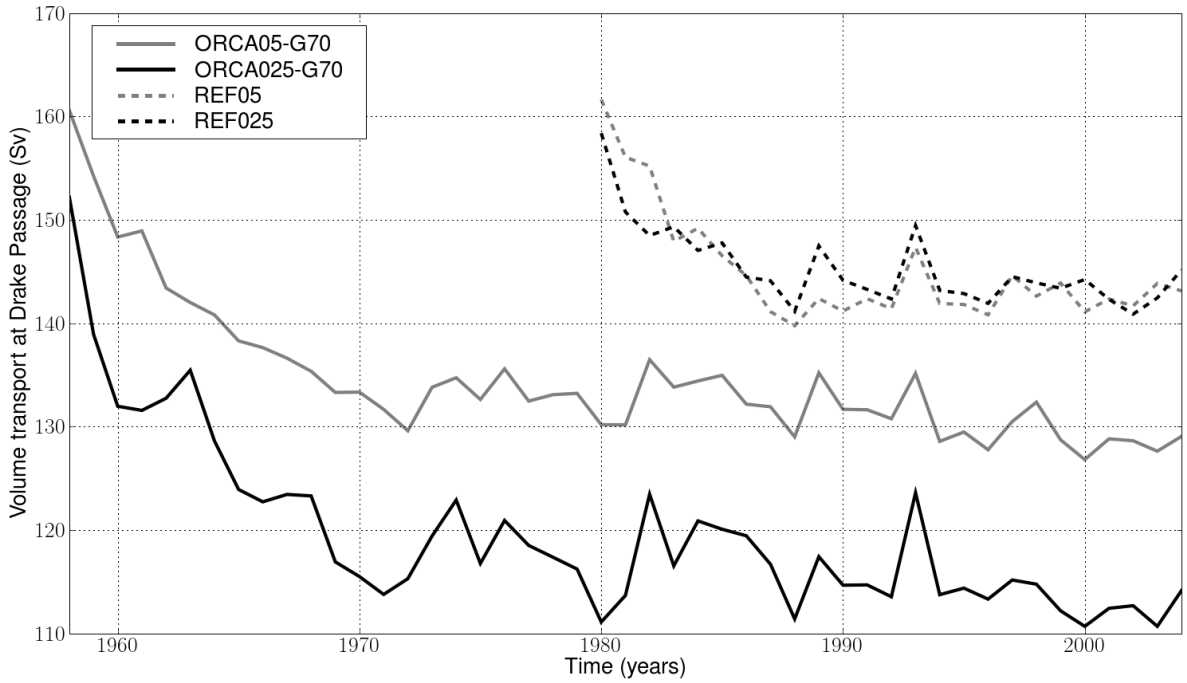

FIG. 3. Time series of annual mass transport at Drake Passage (in Sv) for the DRAKKAR global simulation at 0.5° (grey solid line), the DRAKKAR global simulation at 0.25° (black solid line), the regional reference simulation at 0.5° (dash grey line) and the regional reference simulation at 0.25° (balck dashed line).

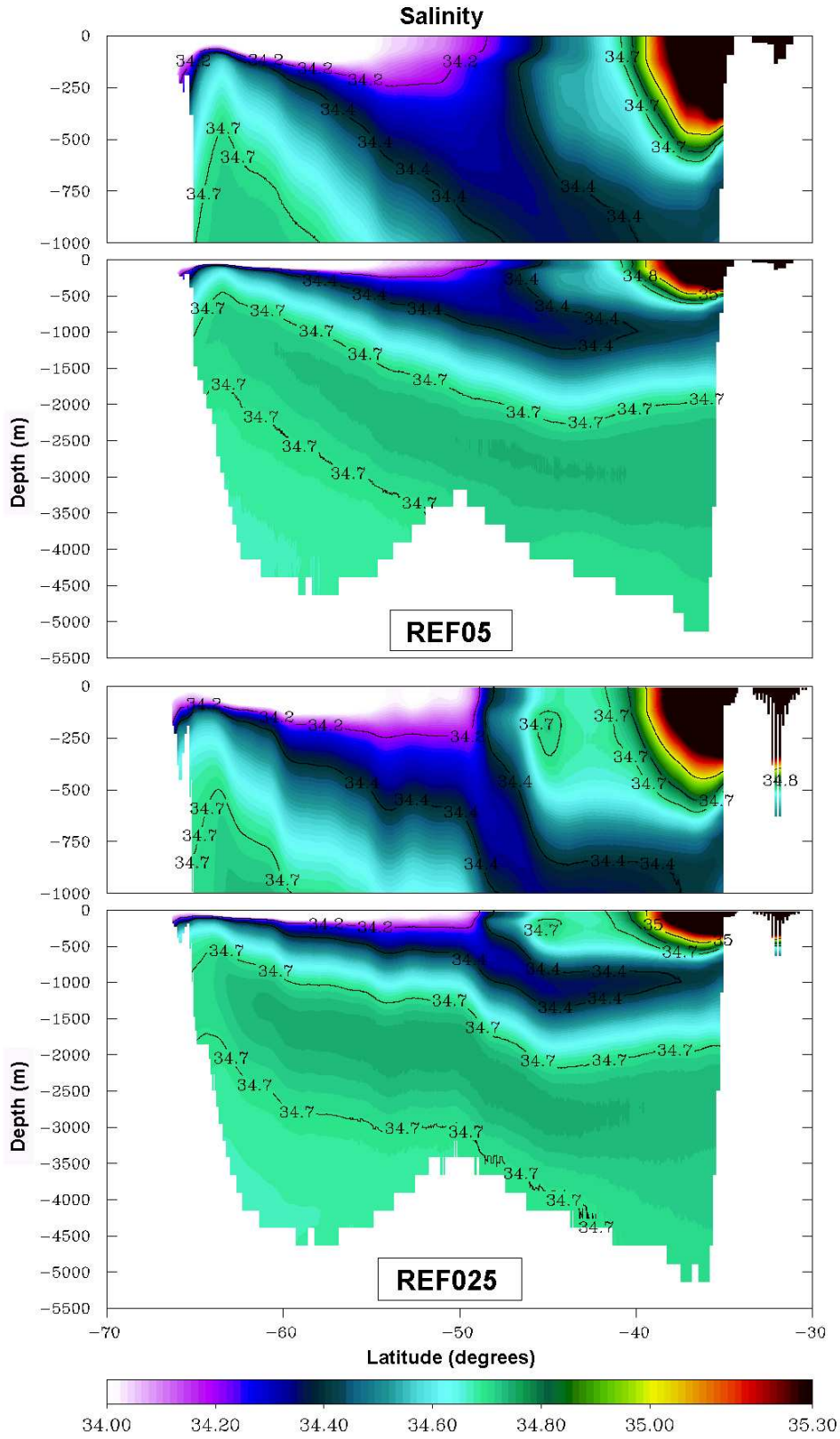

FIG. 4. Mean salinity (1995-2004) along the 115°E cross-section in the REF05 simulation (top panel) and the REF025 simulation (bottom panel) with a zoom on the upper 1000 m. Solid black contours indicate some surface referenced isopycnals. The colorbar indicates salinity in psu units.

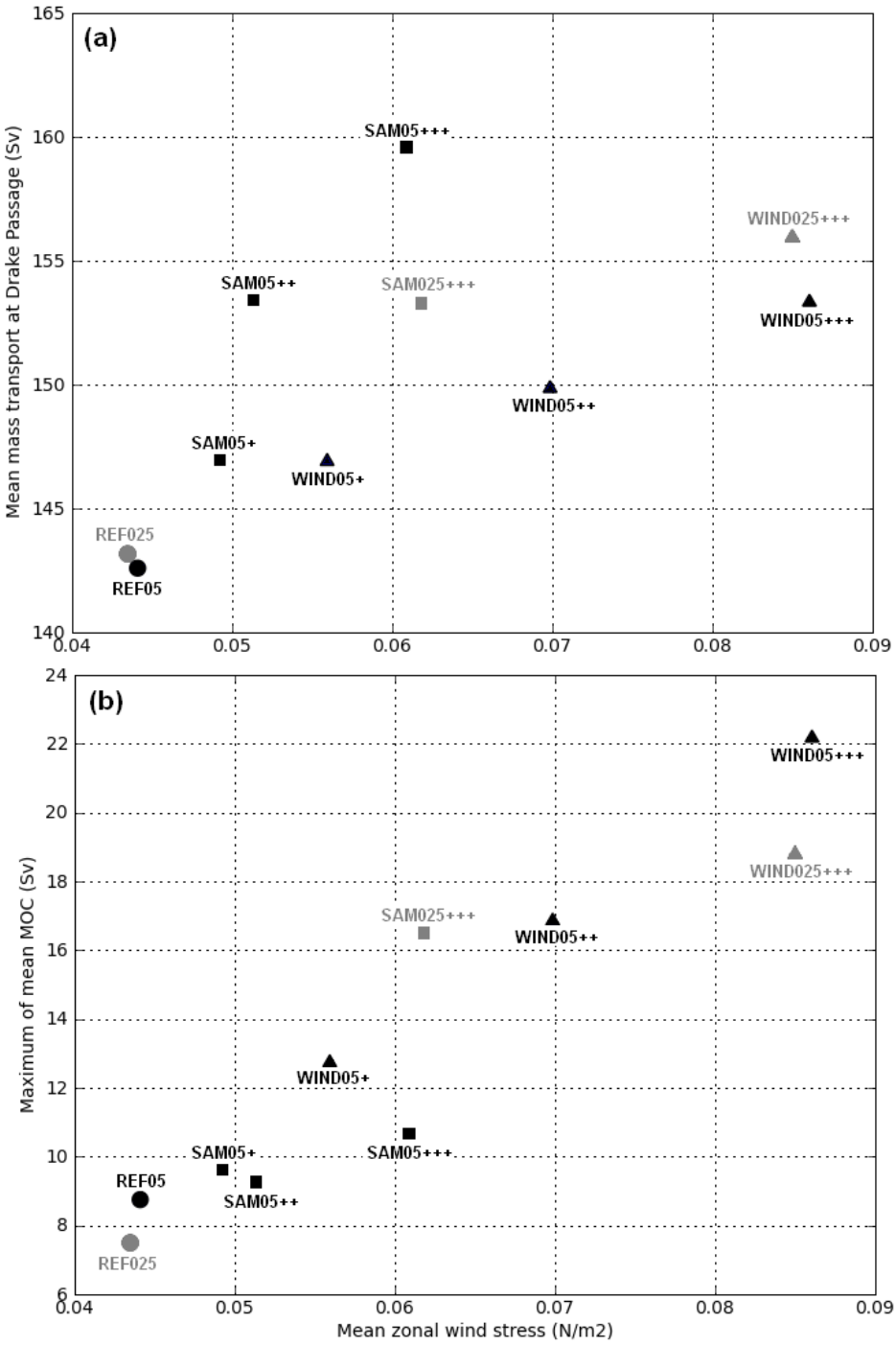

FIG. 5. (a) 1995-2004 mean mass transport at Drake Passage (in Sv) and (b) maximum of the 1995-2004 subpolar cell between 40°S and 55°S (in Sv) plotted against 1995-2004 mean zonal wind stress in $N.m^{-2}$, for REF simulations (circles), WIND simulations (triangles) and SAM simulations (squares). 0.5° simulations are in black and 0.25° simulations are in grey.

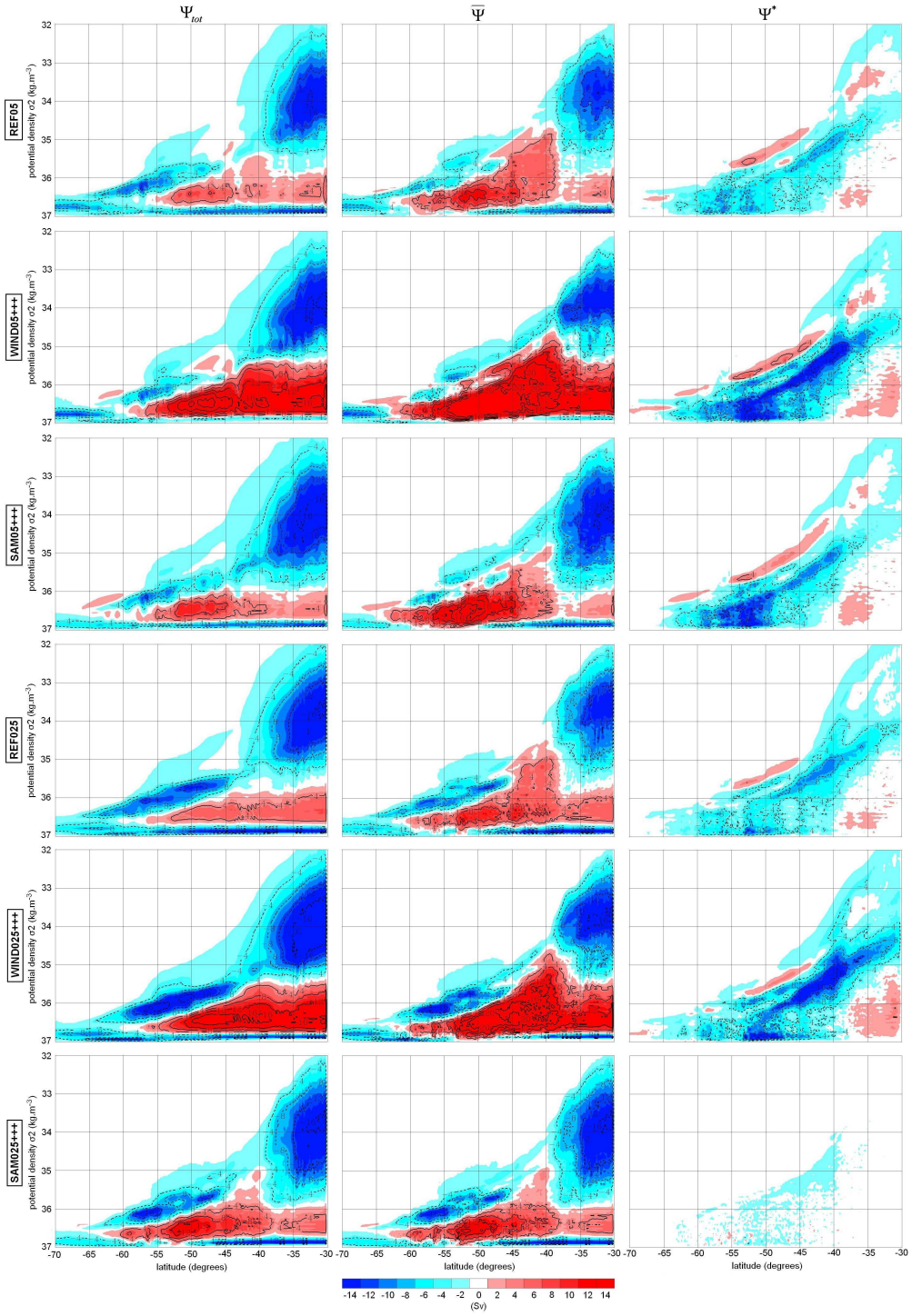

FIG. 6. MOC (in Sv) in σ_2 potential density coordinates: (left) the total circulation Ψ_{tot}, (middle) the Eulerian-mean circulation $\overline{\Psi}$ and (right) the transient eddy-induced circulation Ψ^* for (from top to bottom) REF05, WIND05+++, SAM05+++, REF025, WIND025+++ and SAM025+++ experiments. Red cells correspond to clock-wise flows and blue cells to counter-clockwise flows.

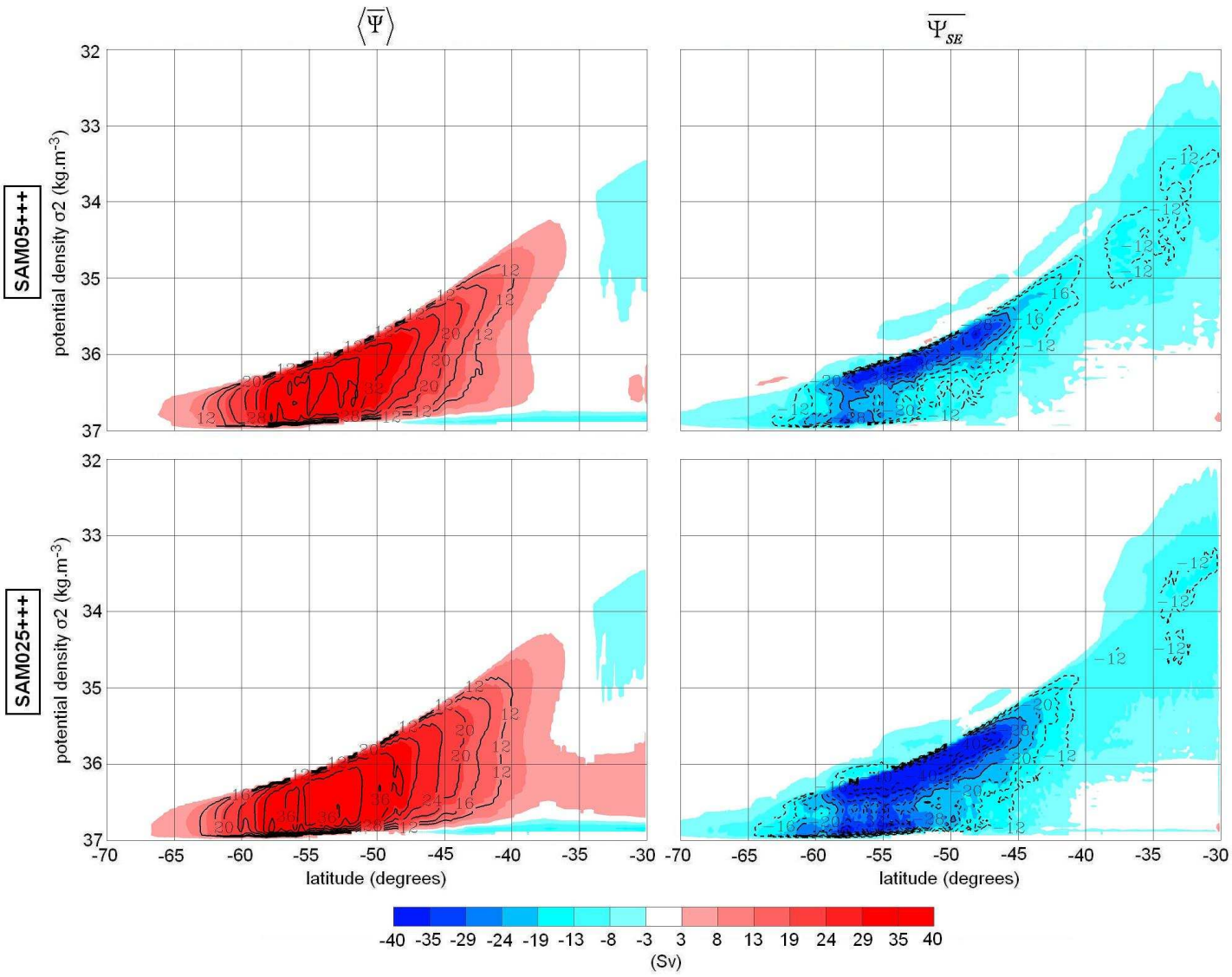

FIG. 7. MOC (in Sv) in σ_2 potential density coordinates: (left) the Eulerian mean circulation zonally averaged $< \overline{\Psi} >$, (right) the standing eddy-driven circulation $\overline{\Psi_{SE}}$ for (from top to bottom) SAM05+++ and SAM025+++ experiments. Red cells correspond to clock-wise flows and blue cells to counter-clockwise flows.

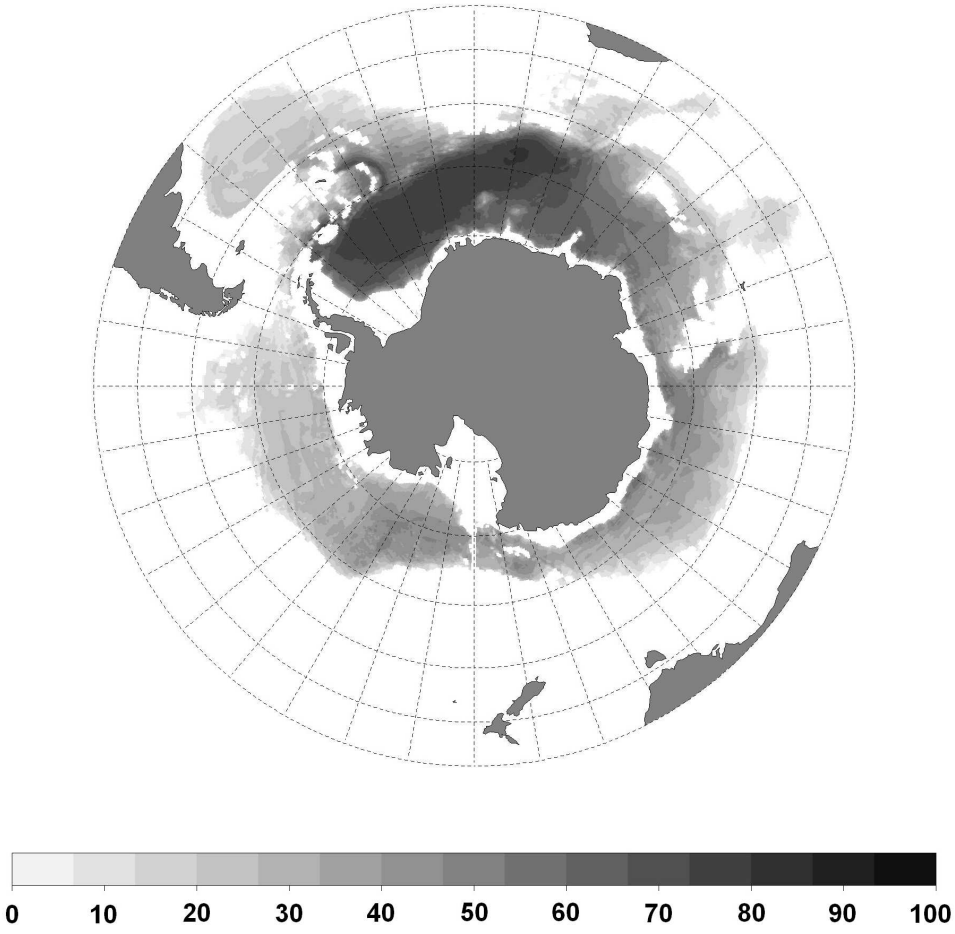

FIG. 8. Percentage of the water depth restored with a time scale of less than ten years. That is to say a total restoring coefficient $\frac{M(x,y,z)}{\tau} > 3,17.10^{-9}\ s^{-1}$, corresponding to a mask coefficient $M(x,y,z) > 0.2$ and a restoring time scale $\tau = 2\ years$.

List of Tables

1 Comparison of grid types (second column) and grid sizes at 60°S (third column) of various model configurations. The Mercator grid is isotropic, i.e., dy is refined as dx decreases poleward. Note that the grid of the UVic ESCM 0.2°x0.4° model is strongly anisotropic (22 km x 44 km). The last column indicates studies on the Southern Ocean sensitivity to winds cited in this paper. 47

2 (columns 2-4) Main characteristics of experiments: horizontal resolution used and corresponding parameters of the synthetic forcing applied. α and β are the constants defined in the equation(1) and $1std(SAM) = 0.993$. (columns 5-7) ACC mean position computed from the PF and the SAF mean positions. An estimation of the shift of the ACC (in degrees) under perturbed winds is computed from the difference between the ACC mean position of control experiments and of perturbed experiments. An estimation of the width of the ACC (in degrees) is computed from the distance between the PF and the SAF mean positions. 48

TABLE 1. Comparison of grid types (second column) and grid sizes at 60°S (third column) of various model configurations. The Mercator grid is isotropic, i.e., dy is refined as dx decreases poleward. Note that the grid of the UVic ESCM 0.2°x0.4° model is strongly anisotropic (22 km x 44 km). The last column indicates studies on the Southern Ocean sensitivity to winds cited in this paper.

Model	*Grid type*	*dy*	*Reference*
ORCA2-LIM	Mercator	50 km	(Lefebvre and Goose 2005)
PERIANT05	**Mercator**	**28 km**	-
MESO 1/2°	Mercator	28 km	(Hallberg and Gnanadesikan 2006)
OCCAM 1/4°	lon,lat	27 km	-
UVic ESCM 0.2°x0.4°	lon,lat	22 km	(Spence et al. 2010)
PERIANT025	**Mercator**	**14 km**	-
CM2.4	Mercator	14 km	(Farneti et al. 2010)
MESO 1/4°	Mercator	14 km	(Hallberg and Gnanadesikan 2006)

TABLE 2. (columns 2-4) Main characteristics of experiments: horizontal resolution used and corresponding parameters of the synthetic forcing applied. α and β are the constants defined in the equation(1) and $1std(SAM) = 0.993$. (columns 5-7) ACC mean position computed from the PF and the SAF mean positions. An estimation of the shift of the ACC (in degrees) under perturbed winds is computed from the difference between the ACC mean position of control experiments and of perturbed experiments. An estimation of the width of the ACC (in degrees) is computed from the distance between the PF and the SAF mean positions.

Simulation	*Resolution*	α	β [$std(SAM)$]	*ACC*	*Shift*	*Width*
REF05	0.5°	1	0	51.1°S	-	7.1°
WIND05+	-	1.1	0	50.1°S	1.0°N	5.3°
WIND05++	-	1.2	0	49.7°S	1.4°N	4.8°
WIND05+++	-	1.3	0	49.4°S	1.7°N	4.3°
SAM05+	-	1	0.5	51.3°S	0.2°S	6.6°
SAM05++	-	1	1	50.7°S	0.4°N	5.2°
SAM05+++	-	1	2	50.9°S	0.2°N	4.9°
REF025	0.25°	1	0	50.3°S	-	5.7°
WIND025+++	-	1.3	0	49.2°S	1.1°N	4.1°
SAM025+++	-	1	2	50.6°S	0.3°S	5.3°